Geopersia 2026, 16(1): 229-251
DOI: 0.22059/geope.2025.400343.648837

RESEARCH PAPER

# Using mineral chemistry in thermobarometry and thermo-oxybarometry of Fe-Ti±P host mafic-ultramafic rocks in the XV deposit (Bafq area, Central Iran): Implications for tectonic setting and magma nature

**Sakine Amraei [1], *, Mohammad Yazdi [1], Mehrdad Behzadi [1], Majid Ghasemi Siani [2], Hamed Ebrahimi Fard [2], Liang Qiu [3], Chang Zhi Wu [4], Minghua Ren [5], Shahrokh Rajabpour [6]**

[1]Department of geology of ore minerals and groundwater resources, Shahid Beheshti University, Tehran, Iran

[2] Department of Geochemistry, Faculty of Earth Sciences, Kharazmi University, Tehran, Iran

[3] State Key Laboratory of Geological Processes and Mineral Resources, School of Earth Sciences and Resources, China University of Geosciences, Beijing 100083, China

[4] School of Earth Sciences and Resources, Chang'an University, Xi'an, China

[5] Department of Geoscience, University of Nevada, Las Vegas, Las Vegas, NV 89154, USA

[6] Instituto de Geología Económica Aplicada (GEA), Universidad de Concepción, Casilla 160-C, Concepción, Chile

Received: 10 August 2025, Revised: 01 December 2025, Accepted: 21 December 2025

**Abstract**

The Fe-Ti ± P oxide mineralization hosted by the XV intrusion is located within the Bafq-Saqand metallogenic province in western Central Iran. This mineralization occurs in gabbroic and pyroxenitic rocks and appears in semi-massive, net-textured, and disseminated forms. According to the Ti + Cr + Na versus Al discrimination diagram, the analyzed pyroxenes are of igneous origin. Classification on the Q (Ca + Mg + Fe2+) versus J (2Na) diagram places them within the Ca-Fe-Mg pyroxene group (Quad). The average Mg# [Mg/(Mg + Fe2+) × 100] values are 87.23 wt.% for gabbroic and 84.20 wt.% for pyroxenitic pyroxenes. CaO contents range from 13.30 to 23.00 wt.% in gabbroic samples and from 18.52 to 23.12 wt.% in pyroxenitic rocks. In the Ca + Na(B) (a.p.f.u) versus Na(B) (a.p.f.u) diagram, the studied amphiboles are classified as calcic. Thermobarometric calculations indicate that the gabbros crystallized at temperatures between 904-1230 °C under pressures of 8.0-10.3 kbar, whereas the pyroxenites formed under slightly lower thermal conditions (901-1180 °C) and pressures from 7.0 to 8.9 kbar. Coexisting titanomagnetite-ilmenite mineral pairs record cooling temperatures ranging from 448 °C to 727 °C, mainly within 554-645 °C, with oxygen fugacity ($f$O2) values from -17.28 to -23.96. The relatively high $f$O2 values suggest that the parental magma evolved under oxidizing conditions, likely associated with an extensional tectonic setting during emplacement, cooling, and fractional crystallization.

**Keywords:** Geochemistry, Geothermometry, Oxybarometry, magma Nature, Central Iran.

## Introduction

The processes involved in rock formation within magmatic systems require reliable quantitative estimates of the temperature and pressure conditions during crystallization, as these parameters govern both the depth and the evolution of the magma body (Rutter et al., 1989). Mineral

* Corresponding author e-mail: S.amraei.ac.ir@gmail.com

chemistry-particularly that of amphibole and pyroxene-provides one of the most robust approaches for inferring these parameters, as numerous studies (e.g., Molina et al., 2009) have demonstrated strong correlations between mineral composition and the overall chemistry of the host rock. Amphibole and pyroxene are significant constituents of gabbroic assemblages, and their aluminum content reflects crystallization pressure and temperature (Hammarstrom & Zen, 1986; Aoki & Shiba, 1973). Amphibole, in particular, forms over a wide range of temperatures and pressures (Hammarstrom & Zen, 1986), and its composition is highly sensitive to the depth of magma emplacement, especially in H2O-rich magmas (Murphy et al., 2012).

The aluminum content of calcic amphiboles correlates strongly with pressure and depth of formation (Hammarstrom & Zen, 1986), while their chemical variability also reflects the evolving composition of the melt and the presence of coexisting phases. In certain gabbros, the abundance of amphibole may result from direct crystallization of hydrous basaltic magma (Wan et al., 2013) or from reactions among early-formed minerals and water rich residual melts (Yan et al., 2015). Hence, amphibole composition serves as a key petrogenetic indicator for estimating crystallization conditions, with temperatures ranging from approximately 400 to 1150 °C and pressures ranging from less than 1 to 23 kbar (Yavuz & Doner, 2017). Its close association with plagioclase makes amphibole-plagioclase thermometry a powerful tool for evaluating magmatic temperature (Helmy et al., 2004; Blundy & Cashman, 2008). Gabbroic and pyroxenitic systems worldwide constitute significant hosts of Fe-Ti±P mineralization. Several geothermometers have been calibrated for such magmatic environments, including clinopyroxene-ilmenite (Bishop, 1980), clinopyroxene (Kretz, 1994; Putirka, 2008), amphibole-clinopyroxene (Ridolfi & Renzulli, 2010, 2012), plagioclase (Nekvasil, 1992), amphibole (Helz, 1973; Putirka, 2016), and amphibole-plagioclase (Schmidt, 1992; Stein & Dietl, 2001).

Oxygen fugacity ($fO_2$) is another fundamental parameter of magmatic systems that influences phase equilibria (Lindsley & Frost, 1992; Brzozowski et al., 2021; Mokchah & Mathieu, 2022) and governs the partitioning of ore forming metals between melt and fluid phases (Jugo et al., 1999), thereby affecting mineralization potential (Blevin et al., 1996). Thermo-oxybarometry based on Fe-Ti oxides remain one of the most widely used approaches to estimate $fO_2$ in intermediate to silicic magmas (Buddington & Lindsley, 1964; Carmichael, 1967; Andersen & Lindsley, 1988; Ghiorso & Sack, 1991; Lattard et al., 2005; Ghi orso & Evans, 2008). The Fe-Ti oxide thermometer and oxybarometer rely on temperature dependent redox equilibria between titanomagnetite (magnetite-ulvospinel solid solution) and ilmenite-hematite solid solution. These parameters help reconstruct crystallization and re-equilibration conditions and are crucial for deciphering oxidation-reduction states, magmatic differentiation, contamination, and mixing processes (Lattard et al., 2005).

The XV Fe-Ti ± P oxide deposit, located in the western Posht-e-Badam Block (PBB) within the Bafq-Saghand Metallogenic Province (BSMP) (Amraei et al., 2021; 2024a, b, 2025), is one of the region's key intrusive bodies. Despite extensive geological and mineralogical studies in the Bafq-Saghand area, the physicochemical conditions under which the XV intrusion crystallized-including temperature, pressure, oxygen fugacity, and magma emplacement depth-are still poorly understood, which is the main focus of this study. The absence of integrated quantitative data linking silicate and oxide mineral chemistry introduces uncertainty about the magmatic evolution and redox conditions that control Fe-Ti mineralization in the system.

This research aims to utilize electron microprobe data from silicate and oxide minerals to determine the geothermobarometric conditions and physicochemical characteristics of the XV primary magma, including temperature, pressure, and oxygen fugacity during crystallization. Magnetite-ilmenite thermo-oxybarometry is used to define the thermal and redox conditions of the XV rocks, estimate the depth at which the magma was emplaced and underwent fractionation, and clarify the tectonic setting and petrogenetic development of the XV intrusion. This analysis also refines the Fe-Ti oxide mineralization model for the deposit. Overall, the study tackles the challenge of quantitatively determining the crystallization conditions (P-T-$f$O2) and emplacement depth of the XV Fe-Ti bearing intrusion. Addressing this is crucial for understanding magmatic differentiation, oxidation state, mineralization potential, and for establishing geochemical criteria for exploring Fe-Ti-P deposits in continental back-arc provinces such as the BSMP.

## Regional Geology

A series of dextral strike-slip faults divides the Central Iranian Microcontinent (CIMC) into the Yazd, PBB, Tabas, and Lut blocks toward the east (e.g., Aghanabati, 2013) (Fig. 1a). The PBB forms a broad tectonic arc situated between the Tabas and Yazd blocks (Figs. 1 & 2) and consists of metamorphic, igneous, and sedimentary units (Ramezani & Tucker, 2003; Rajabi et al., 2012). The PBB is underlain by Neoproterozoic metamorphic rocks of the Chapedony, Boneh-Shurow, and Posht-e-Badam complexes, along with the Tashk Formation (Fig. 1b), which are overlain by Mesozoic and Cenozoic sedimentary sequences.

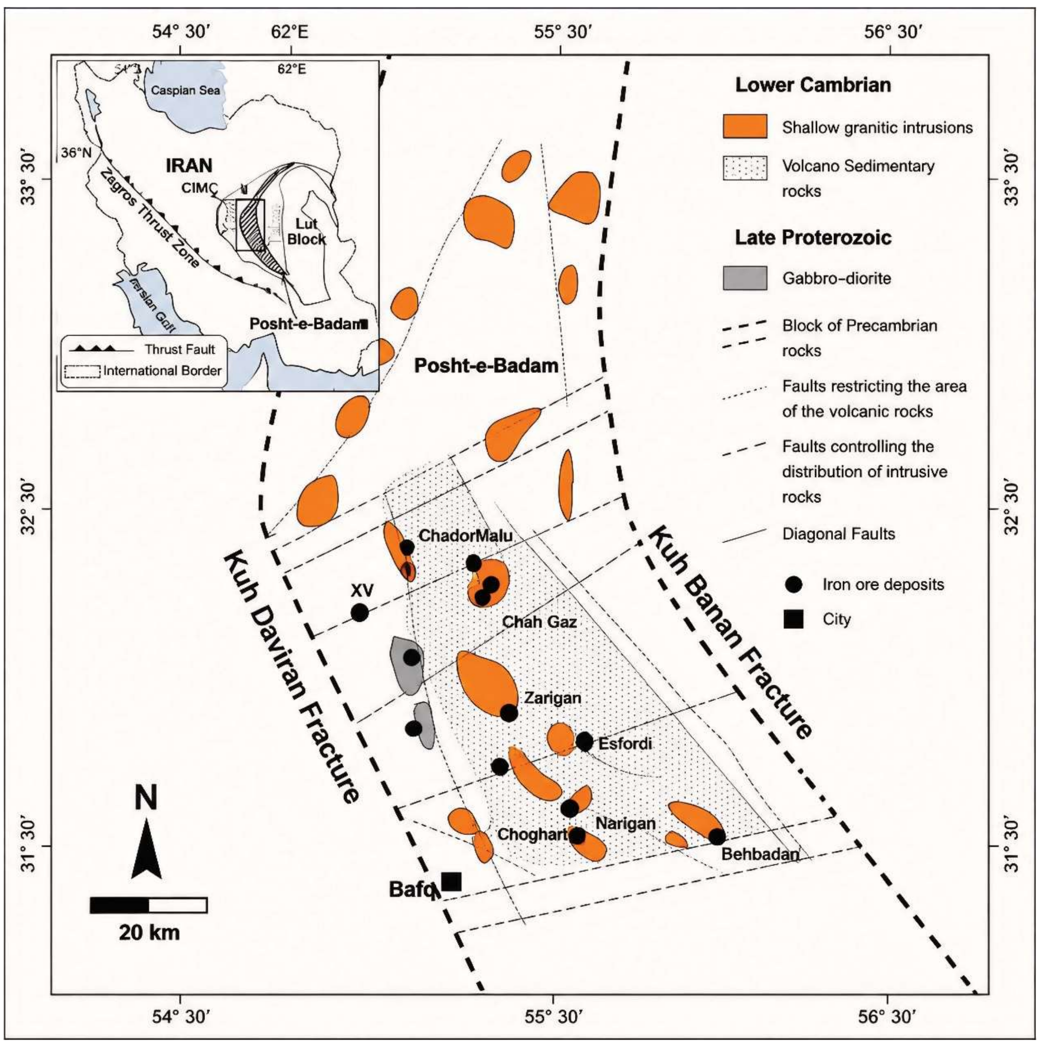


**Figure 1.** The distribution of iron oxide-apatite (IOA) deposits, and XV intrusion within the intrusive units of the Posht-e-Badam volcanic-intrusive belt, as modified from Heidarian et al. (2018)

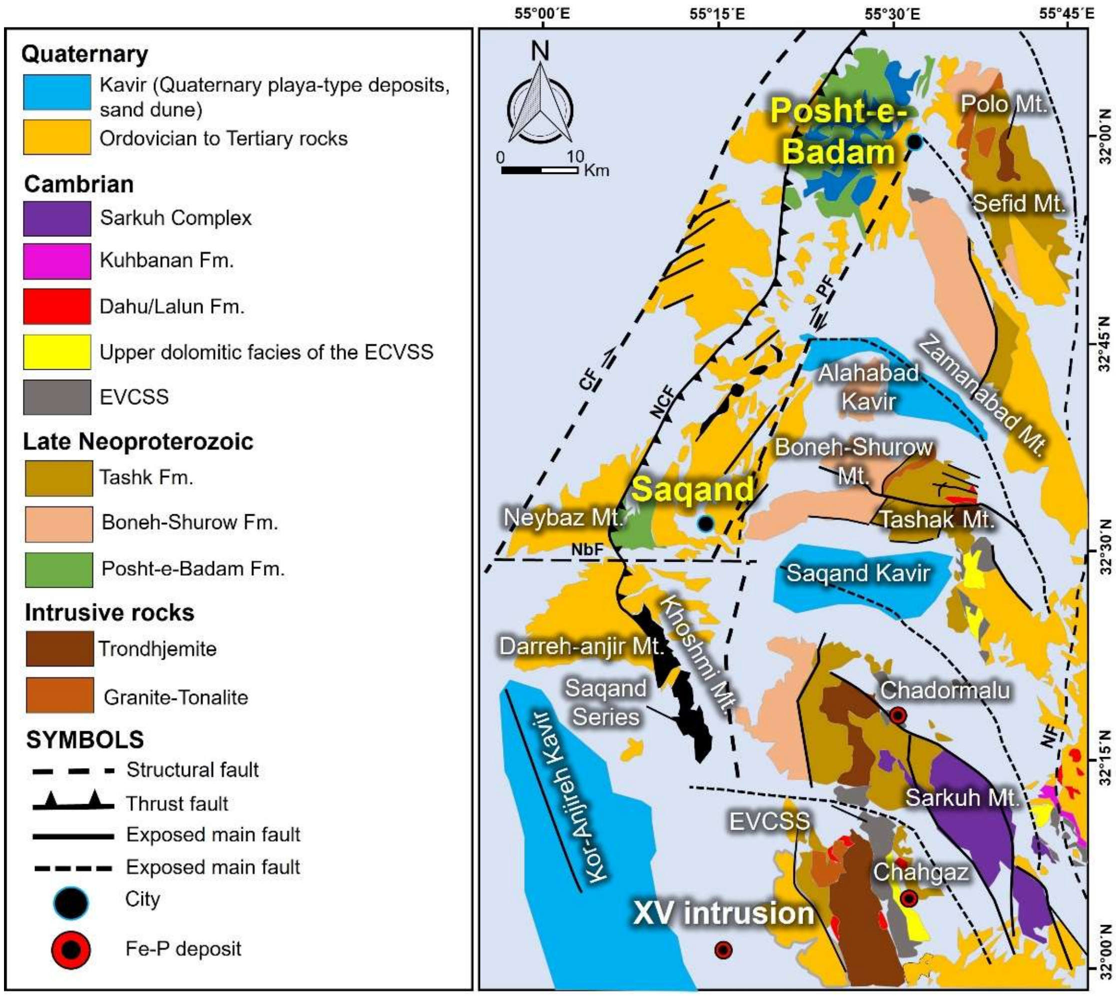

**Figure 2.** Geological map of the PBB and location of XV intrusion (Modified after Rajabi et al, 2015).

The Precambrian basement consists of mid- to high-grade metamorphic rocks from the Late Neoproterozoic era, classified into the Boneh-Shurow and Posht-e-Badam complexes (Ramezani & Tucker, 2003) (Fig. 1b). The Chapedony Complex, dating from 502 to 616 Ma based on zircon U-Pb ages (Ramezani & Tucker, 2003), represents the oldest known basement in Iran. It mainly includes high-grade gneisses and migmatites associated with granolithic facies (Ghazi et al., 2020). Eocene granodioritic bodies, such as the Darreh Anjir and Khoshoumi intrusions, cut through this complex (Ghazi et al., 2020). The Boneh-Shurow Complex, with zircon U-Pb ages ranging from 617 to 535 Ma (Ramezani & Tucker, 2003), reaches about 2 km in thickness and features a variety of metamorphic rocks, including gneiss, micaschist, amphibolite, dolomitic marble, granite gneiss, and localized mafic lithologies. These units are mainly found along the eastern margin of the Posht-e-Badam fault (Ramezani & Tucker, 2003; Aghanabati, 2013; Ghazi et al., 2020) (Fig. 1b). Above the metamorphic basement lies the Tashk Formation, with zircon U-Pb ages between 602 and 617 Ma (Ramezani & Tucker, 2003). The Tashk Formation includes a wide variety of rocks, such as greenstones, schists, metagreywackes, marbles, gneisses, amphibolites, pyroxenites, serpentinites, metabasites, and conglomerates (Ghazi et al., 2020; Amraei et al., 2024a, 2024b) (Fig. 1b). It is the main Precambrian basement unit of the Bafq district and features low- to high-grade metamorphic rocks such as slates, shales, quartzites, sandstones, greywackes, and phyllites. Located west of the Posht-e-Badam fault, this formation is also intruded by Triassic granitic bodies (Ramezani & Tucker, 2003).

The Sarkuh Complex features highly foliated mica schists found within the upper amphibolite facies (Ghazi et al., 2020). During the Early Cambrian, approximately 2,000 to 2,500 meters of volcanic and felsic to intermediate volcano-sedimentary rocks were deposited, forming the Early Cambrian volcano-sedimentary sequence (ECVSS). These rocks include an interlayered succession of conglomerates, sandstones, mafic to felsic volcanic units, black pyritic clays and shales, volcaniclastic beds, tuffaceous shales, and carbonates, with zircon U-Pb ages ranging from 554 to 529 Ma (Ramezani & Tucker, 2003) (Fig. 1a). In the PBB, younger formations—especially those from the Late Cambrian to Ordovician—are rarely exposed, while Mesozoic and Neogene rocks are more widespread (Fig. 1b). In the eastern part of the district, Jurassic strata mainly from the Shemshak Formation are visible, whereas Cretaceous sequences dominate the western sector (Rajabi et al., 2015). Eocene sedimentary layers are overlain by Oligocene red beds and younger Pliocene-Pleistocene conglomerates (Ramezani & Tucker, 2003). The mafic groups within the PBB consist of volcanic flows, late-stage dolerite dykes, subvolcanic gabbro bodies, and gabbro-diorite intrusions (Rajabi et al., 2015; Poshtkoohi et al., 2018; Ghazi et al., 2020). These units mainly intrude the Rizu Formation of Early Cambrian age, indicating that magmatic activity postdates its deposition.

## Geology of the XV Intrusion

Field observations indicate that the magnetic XV deposit is associated with a ribbon-shaped mafic-ultramafic intrusive body trending northwest-southeast, covering approximately 22 $km^2$. The intrusion, dated at $363 \pm 67$ Ma based on apatite U-Pb ages (Amraei et al., 2024b), is situated within Late Neoproterozoic to Early Cambrian units of the Rizu Series at depths of approximately 150-400 m beneath the surface and is overlain by Tertiary conglomerates and Quaternary sediments. The intrusive body exists in a flat, desert-like terrain, where only Late Proterozoic rocks are exposed at the XV site, a few kilometers east of the intrusion. These host rocks include gneisses, schists, granite-gneiss, and other metamorphic lithologies, such as interlayered sequences of metamorphosed mafic-ultramafic rocks.

## Petrography and Mineralography

The XV intrusion primarily consists of medium-grained cumulate gabbro and pyroxenite (Fig. 3). The gabbro, which displays a gray to dark-green color, represents the major component of the intrusion (Fig. 4a). The dominant textures of the XV rocks are granular, cumulate, and poikilitic, and they contain variable proportions of clinopyroxene, plagioclase, and amphibole, accompanied by intercumulus opaque minerals and apatite (Fig. 4b, c). In the gabbroic units, plagioclase (25–30 vol%; 0.5–1 mm) occurs as euhedral to subhedral crystals. Although most plagioclase grains appear fresh, partial alteration to sericite and clay minerals is evident in some grains (Fig. 4b, c). Clinopyroxene (20–30 vol%; 0.3–0.5 mm) and amphibole (15–20 vol%; 0.3–0.7 mm) occur as primary crystals (Fig. 4c). Opaque minerals occur interstitially between the primary silicates. Secondary amphibole formed along reaction rims where silicate crystals are in contact with opaque minerals (Fig. 4c). Pyroxenite alternates with gabbroic layers and exhibits granular to poikilitic textures (Figs. 3 and 4d).

The primary crystals—mainly pyroxene and amphibole—are commonly corroded at their contacts with opaque minerals and typically show rounded margins (Fig. 4f). Clinopyroxene (60–70 vol%; 0.8–1.5 mm) is the dominant mineral phase in the pyroxenite (Fig. 4e, f). Plagioclase (~10 vol%; <0.3 mm) is generally altered, whereas clinopyroxene commonly shows strong serpentinization and chloritization along fractures (Fig. 4e). Amphibole (5–10 vol%; 0.3–0.5 mm) occurs as euhedral to subhedral crystals, but in highly altered samples, it is partially replaced by chlorite, calcite, and epidote (Fig. 4d).

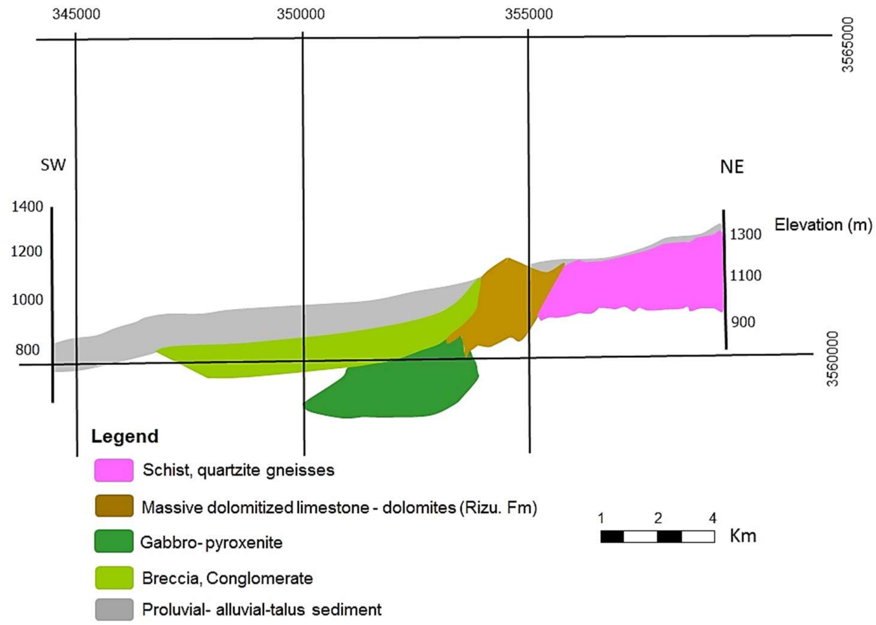


**Figure 3.** Cross-sections of the XV intrusion and surrounding host rocks, oriented along the WSW-ENE direction

Interaction between silicates and opaque minerals has produced marginal bands of hornblende (Fig. 4e, f). In both rock types, opaque minerals and apatite occupy the interstitial spaces among earlier-formed silicates (Fig. 4f). The opaque minerals consist mainly of titanomagnetite and ilmenite, with minor pyrite and chalcopyrite.

Three main textural types of Fe–Ti mineralization are recognized: (I) disseminated ore, occurring as irregular to euhedral grains ranging from <0.2 mm to 2–3 mm in size (Fig. 5a, b); (II) ilmenite–titanomagnetite intergrowths (Fig. 5c, d), in which the contact between ilmenite and titanomagnetite is typically smooth, although locally irregular or curved boundaries are observed; and (III) blade-shaped ilmenite inclusions within titanomagnetite, formed by exsolution of the ulvöspinel component from Ti-rich magnetite at high temperature (Haggerty, 1991) (Fig. 5e, f). The ilmenite–titanomagnetite intergrowths occur as intercumulus aggregates enclosed within cumulate silicates, mainly plagioclase and pyroxene.

In mineralization types II and III, titanomagnetite–ilmenite networks occur as lamellae formed through rapid oxidation of primary solid solutions. The interwoven ilmenite–magnetite structure—often described as stockwork or sandwich texture—shows variable blade thickness (Haggerty, 1991). Martitization texture is common in some titanomagnetite crystals (Fig. 5h) and generally develops along the {111} planes of titanomagnetite, indicating low-temperature oxidation under high oxygen fugacity, particularly in shallow samples (Fig. 5g, h). Most ilmenite grains show no hematite exsolution lamellae and are nearly pure (Fig. 5i). Sulfide inclusions, predominantly pyrite, are also observed within the oxide minerals (Fig. 5i).

## Analytical method

A comprehensive mineralogical study of oxide mineral pairs (magnetite-ilmenite) was performed on ten polished thin sections to assess oxygen fugacity, temperature, and pressure conditions. Geochemical data from a previous study (Amraei et al., 2024a), collected via an independent analytical method, were also included to improve the geothermobarometric estimates. Electron microprobe analyses were conducted at the University of Nevada, Las Vegas, using a JEOL JXA-8900 instrument equipped with four wavelength dispersive spectrometers (see Appendix Tables a-e).

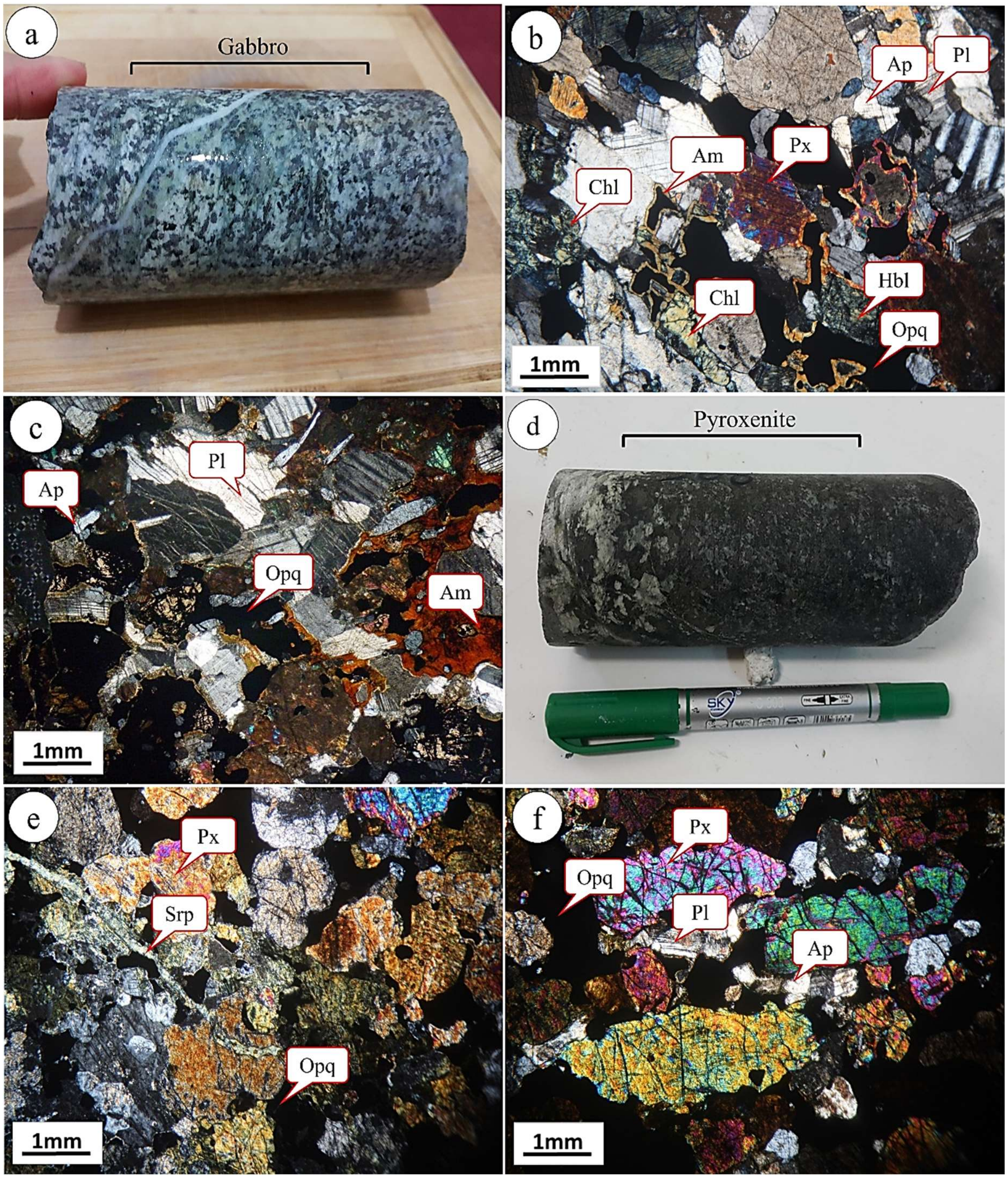


**Figure 4.** a) Images of drilling cores from the gabbroic host units of XV deposit Fe-Ti oxides, b) reaction rim between silicate minerals and oxide minerals in the mineralized gabbro, c) alteration of pyroxene into amphibole in contact with ilmenite crystals in the mineralized gabbro, d) Images of drilling cores from the pyroxenite host units of XV Fe-Ti deposit, e) Pyroxene and plagioclase minerals with rounded rims in the pyroxenite, and f) Cumulative texture resulting from the accumulation of pyroxene and plagioclase in the pyroxenite. Abbreviations: Hbl: hornblende, Am: secondary amphibole, Px: pyroxene, Pl: plagioclase, Srp: serpentine, Chl: chlorite, Ser: sericite, Opq: opaque mineral

Analytical conditions comprised an accelerating voltage of 15 kV, a beam current of 10 nA, and a beam diameter of 10 µm. Counting times were 30 s for peaks and 15 s for background measurements. The accuracy for major element concentrations is estimated at approximately ± 0.05%. Standard reference materials from the Smithsonian Institution were used to calibrate elements in felsic and oxide minerals, including plagioclase, corundum, chromite, ilmenite, Cr-rich augite, microcline, apatite, and pure metal standards of vanadium and nickel. Elemental calibration and internal quality control followed established microanalytical protocols and continuous verification against Smithsonian microprobe standards, ensuring analytical precision throughout the dataset. Temperature and oxygen fugacity ($f$O2) values were calculated using the ILMAT program (Lepage, 2003). The Fe3+/Fe2+ ratios and total iron corrections followed the procedure of Carmichael (1967). Molar proportions, temperature, and oxygen fugacity were further determined using four thermodynamic models-Anderson (1968), Lindsley (1982), Stormer (1983), and Petrik et al. (2003)-implemented through ILMAT version 1/2 (Lepage, 2003).

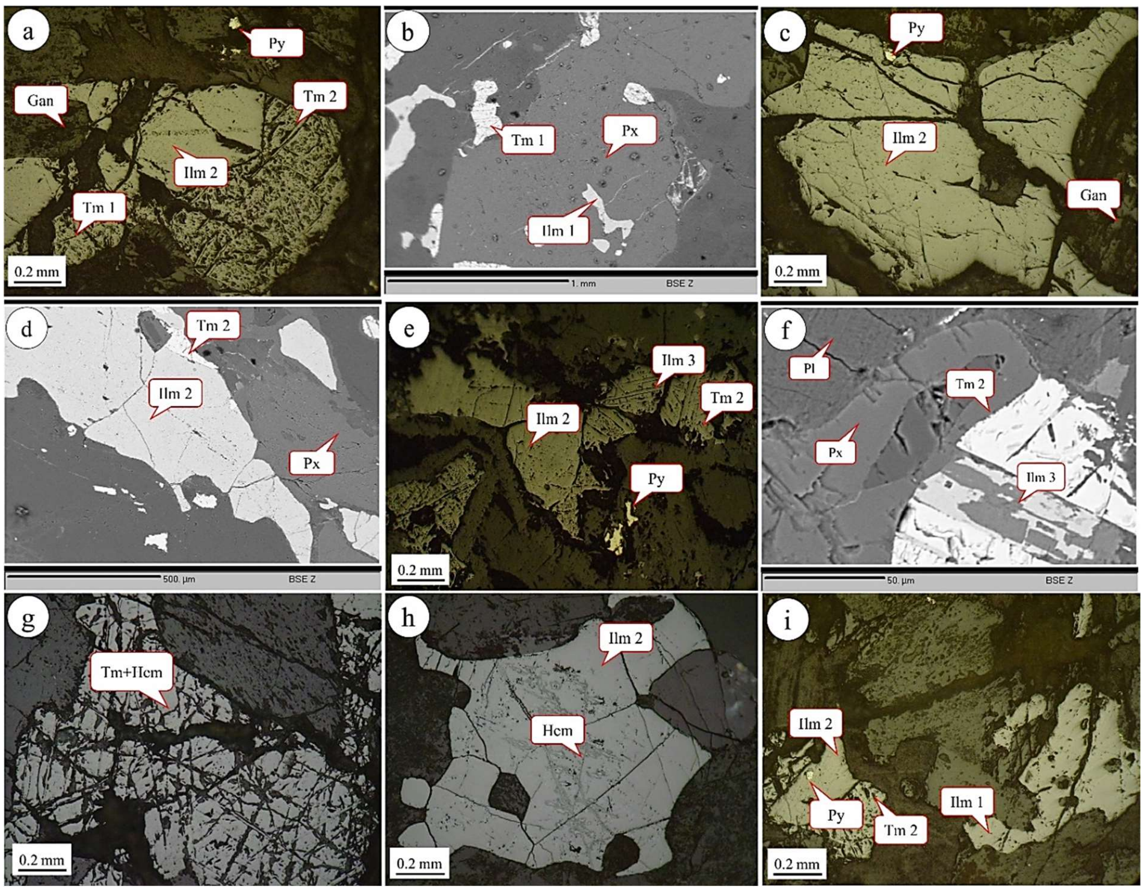


**Figure 5.** Reflected light microscopic and BSE electron microprobe images of Fe-Ti oxide mineralization in XV intrusion. a) Disseminated ilmenite and titanomagnetite (sample. No; BH15-5, 340m), b) Disseminated (Type I) and co-growth (Type II) of ilmenite and titanomagnetite crystals (sample. No; BH15-1, 462m), c) Co-existing ilmenite and titanomagnetite, rounded sulfide minerals (mainly pyrite) were observed (sample. No; BH15-1, 388m), d) Co-growth of ilmenite and titanomagnetite crystals observed side by side with a clear and straight boundary (sample. No; BH15-2, 278m), e) Ilmenite and titanomagnetite with curved border with thin and thicker ilmenite blades in titanomagnetite (sample. No; BH15-3, 460m), f) Type III ilmenite lamellae of variable thickness in a titanomagnetite crystal (sample. No; BH15-4, 488m), g) Martitized titanomagnetite (sample. No; BH15-3, 228m; h) Hematite blades formed in some ilmenite crystals, (sample. No; BH15-2, 248m) and i) The presence of rounded sulfide inclusions (mainly pyrite) in oxide minerals (sample. No; BH15-3, 340m). Abbreviations are adapted from Whitney & Evans (2010). Ilm: ilmenite, Tm: titanomagnetite, Gt: goethite, Gan: gangue mineral or waste, Py: pyrite, Cpy: chalcopyrite, Hem: hematite, Pl: plagioclase, Px: pyroxene, Am: amphibole

## Results

### *Mineral chemistry*

*Pyroxene*: Pyroxenes in the XV rocks are compositionally classified as diopside with minor augite (Amraei et al., 2024a). According to the Ti + Cr + Na vs. Al discrimination diagram proposed by Berger (2005), the analyzed pyroxenes are of igneous origin (Fig. 6a). Classification on the Q (Ca + Mg + $Fe^{2+}$) vs. J (2Na) diagram (Morimoto, 1988) places them within the Ca-Fe-Mg pyroxene group (Quad) (Fig. 6b). Based on the Wo-En-Fs ternary diagram (Morimoto, 1988), pyroxenes from both gabbroic and pyroxenitic rocks predominantly fall within the diopside field, with a minor extension toward the augite field. Their compositional ranges are $Wo_{46.5-39.3}En_{47.5-38.8}Fs_{23.1-12.0}$ in gabbroic rocks and $Wo_{46.0-39.3}En_{45.6-39.9}Fs_{16.2-11.8}$ in pyroxenitic rocks (Fig. 6c). The average Mg# [Mg/(Mg + $Fe^{2+}$) × 100] values are 87.23 for pyroxenes from gabbroic rocks and 84.20 for those from pyroxenitic rocks. CaO contents range from 13.30 to 23.00 wt.% in gabbroic samples and from 18.52 to 23.12 wt.% in pyroxenitic rocks (Appendix Table a) (Amraei et al., 2024a).

*Amphibole*: Amphiboles in the XV rocks range mainly from pargasite to hastingsite, with tremolite also present (Amraei et al., 2024a). Following the classification framework of Hawthorne et al. (2012), the studied amphiboles fall within the calcic group, with Ca + $Na_{(B)}$ values ranging from 1.630 to 2.740 and $Na_{(B)}$ contents varying between 0.126 and 0.815 (see Appendix Table b; Fig. 6d). Based on the classification scheme of Locock (2014), their compositions include Ti-rich pargasite (Ti = 0.335-0.486 apfu), Ti-rich magnesio-hastingsite (Ti = 0.425-0.451 apfu), and tremolite (Fig. 6e).

*Plagioclase*: Plagioclase compositions in the studied samples range from andesine ($An_{50.15}Ab_{35.64}Or_{0.06}$) to labradorite ($An_{63.72}Ab_{44.51}Or_{7.60}$) in gabbroic rocks, and correspond to labradorite ($An_{69.63-46.63}Ab_{53.40-28.90}Or_{3.30-0.00}$) in pyroxenitic rocks (Amraei et al., 2024a) (Fig. 6f). These compositional variations are indicative of fractional crystallization processes (Appendix Table c).

### *Thermobarometry and Thermo-Oxybarometry*

*Pressure Estimation:* Pressure conditions were determined using the methods of Hammarstrom & Zen (1986), Johnson & Rutherford (1989), Mutch et al., (2016) (Appendix Table b). In gabbroic rocks, amphibole barometry indicated pressures ranging from 8.0 to 10.3 kbar, with an average of 8.69 kbar. In pyroxenitic rocks, calculated pressures vary from 7.0 to 8.90 kbar, with an average of 7.82 kbar. The higher pressures observed in the gabbroic samples are probably due to elevated Al concentrations in amphibole compositions, averaging 2.09 wt.% Al. According to the Ti vs. Al discrimination diagram by Hynes (1982) (Fig. 7a), amphiboles from both rock types plot within the medium-pressure field. Additionally, using the AlTotal vs. Fe2+/(Fe2+ + Mg) diagram of Schmidt (1992), the estimated pressures for both lithologies exceed 7 kbar (Fig. 7b).

*Temperature Estimation*: Temperatures were estimated using geothermometers based on calcium amphibole compositions, following the methods of Putirka (2016). The calculated crystallization temperatures range from 904 to 993 °C for gabbroic rocks and from 901 to 1011 °C for pyroxenitic rocks (Appendix Table b). According to Barclay & Carmichael (2004), Ti-rich amphiboles such as Ti-rich pargasite and magnesio-hastingsite are stable at pressures up to 10 kbar and temperatures below 1100 °C, which aligns well with the calculated conditions.

These temperature estimates are consistent with those reported for similar mafic-ultramafic intrusions, including the Abu Ghalaga Fe-Ti-V oxide-bearing gabbros in the Southeastern Desert of Egypt, which crystallized from ferrobasaltic magmas with tholeiitic affinity at lower temperatures (~1082 °C) and pressures (5.1 kbar) than those recorded for the Korab Kansi intrusion (~1180 °C, 8.3 kbar) (Khedr et al., 2022). Using Soesoo's (1997) pyroxene thermometry, the estimated formation temperatures range from 1150 to 1230 °C for gabbroic rocks and from 1140 to 1180 °C for pyroxenitic rocks (Fig. 7c). Additionally, temperatures calculated from the Fe-Ti oxide mineral pair (ilmenite-titanomagnetite) range between 448 and 727 °C, with the majority falling between 554 and 645 °C. The highest temperatures (703-727 °C) are associated with samples from the gabbroic host rocks.

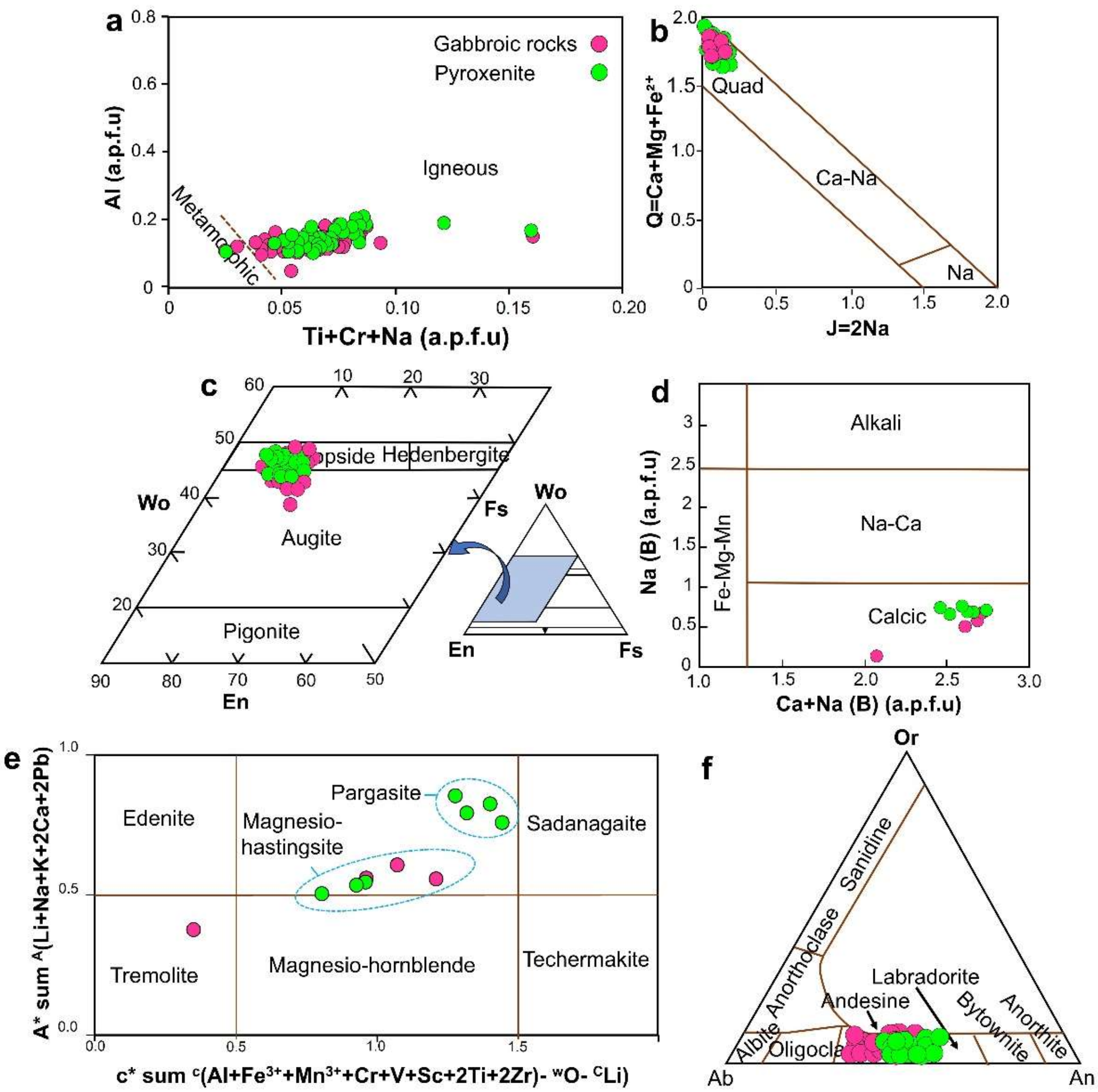


**Figure 6.** Mineral-chemistry classification diagrams for pyroxenes and amphiboles from the XV intrusion: (a) Ti + Cr + Na vs. Al discrimination diagram for pyroxenes after Berger (2005); (b) Q-J classification diagram for pyroxenes after Morimoto (1988); and (c) Composition of pyroxenes from gabbroic and pyroxenite rocks in the Wo-En-Fs triangle diagram (Morimoto, 1988), (d) Composition of amphiboles in gabbroic and pyroxenite rocks of the XV anomaly using the diagram proposed by Hawthorne et al. (2012), (e) Graph of c* sum vs. A* sum (Locock, 2014), (f) Composition of plagioclase of the XV deposit on the orthoclase-albite-anorthite triangular diagram (Deer et al., 2013)

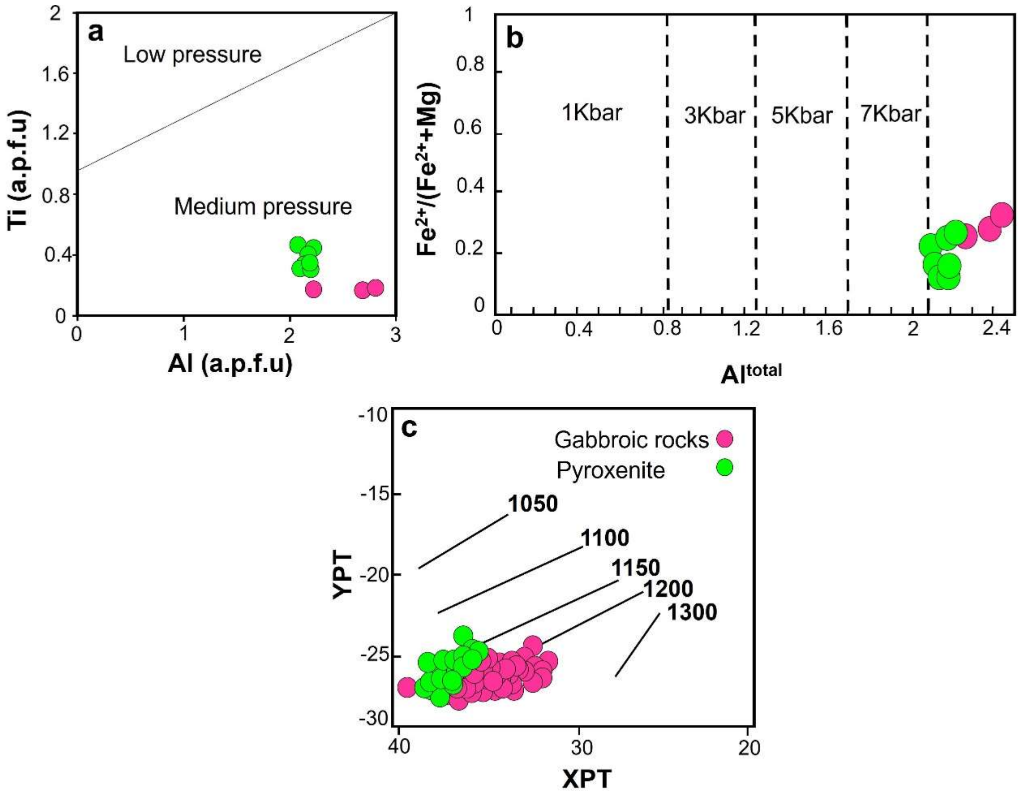


**Figure 7.** a) Amphibole formation pressure, in Ti vs. Al diagram (Hynes, 1982), b) Amphibole composition in gabbroic and pyroxenite units of XV deposit in the diagram of $Al^{Total}$ vs. $Fe^{2+}/(Fe^{2+}+Mg)$ (Schmidt, 1992), c) Determining the crystallization temperature of pyroxenes from the Soesoo diagram (Soesoo, 1997)

**Appendix Table a.** Results of the point analysis of pyroxenes found in gabbroic and pyroxenite rocks from the XV deposit, including data on weight percentages and structural formula calculations based on six oxygen atoms, alongside the determination of their end-member compositions
**Appendix Table b.** Point analysis results of amphiboles in gabbroic and pyroxenite rocks from the XV deposit, including weight percentage data and structural formula calculations based on 23 oxygen atoms, along with the determination of their end-member compositions. The temperatures are reported in degrees Celsius under a pressure of 8.7 kbar
**Appendix Table c.** Results of point analysis of plagioclase in gabbroic and pyroxenite rocks from the XV anomaly, including weight percentage data and structural formula calculations based on 8 oxygen atoms, along with the determination of their end-member compositions
**Appendix Table d.** The results of electron microprobe analysis of titanomagnetite spots. The number of moles of ulvospinel (Usp) has been calculated using (Anderson, 1968). The calculations are based on the number of 4 oxygen atoms

## Discussion

### *Oxygen fugacity and $H_2O$ content of magma*

Oxygen fugacity plays a crucial role in controlling magmatic processes, crystallization sequences, and the mineral assemblages that form within magma (e.g., Botcharnikov et al., 2005). The oxygen fugacity of magma is closely linked to the tectonic environment in which the magma is generated. Magmas produced at convergent plate boundaries typically exhibit relatively high oxygen fugacity, together with elevated Mg and $Fe^{3+}$ contents (Ewart, 1979). In amphibole chemistry, lower oxygen fugacity is commonly associated with higher $Fe^{2+}/(Fe^{2+} + Mg)$ ratios (e.g., Anderson & Smith, 1995; Scaillet & Evans, 1999).

Fe# values between 0.0 and 0.6 indicate high oxygen fugacity, values between 0.6 and 0.8 reflect moderate oxygen fugacity, and values between 0.8 and 1.0 correspond to low oxygen fugacity. In amphiboles from the gabbroic and pyroxenitic rocks of the XV intrusion, Fe# values range from 0.169 to 0.251 and from 0.108 to 0.242, respectively, which is consistent with high oxygen fugacity. Anderson & Smith (1995) suggested that amphiboles with $Al^{IV} > 0.75$ and $Fe^{total}/(Fe^{total} + Mg) > 0.3$ can be used as indicators of oxygen fugacity. In the studied gabbroic and pyroxenitic rocks, the $Fe^{total}/(Fe^{total} + Mg)$ ratios of amphiboles range from 0.184 to 0.285 and from 0.242 to 0.307, respectively, whereas $Al^{IV}$ contents vary from 0.436 to 2.081. When plotted on the $Al^{IV}$ vs. $Fe^{total}/(Fe^{total} + Mg)$ diagram (Fig. 8a), amphiboles from the XV rocks mainly fall within the high-oxygen-fugacity field. Similarly, the $Al^{IV}$ vs. Fe/(Fe + Mg) diagram also places the amphiboles within the high-oxygen-fugacity range (Fig. 8b).

Furthermore, according to the $Al^{VI}$ + 2Ti + Cr vs. Na + $Al^{IV}$ diagram of Schweitzer et al. (1979), the $Fe^{3+}$ content of pyroxenes is a function of oxygen fugacity. Most of the analyzed sample's plot above the $Fe^{3+} = 0$ line, indicating high oxygen fugacity conditions (Fig. 8c). Oxygen fugacity can also be estimated from amphibole composition using the equation proposed by Wones (1989):

$$\log fO_2 = -30930/T + 14.98 + 0.142(P-1)/T$$

The calculated $\log fO_2$ values for amphiboles from the gabbroic and pyroxenitic rocks range from –17.54 to –18.34, with an average of –17.83, and from –17.27 to –17.59, with an average of –17.42, respectively. These values are consistent with relatively high oxygen fugacity. Helz (1973) examined the influence of water content and pressure on mineral chemistry at different depths and proposed that the distribution of aluminum between tetrahedral and octahedral sites in pyroxenes can provide useful constraints on both magma water content and pressure conditions during crystallization.

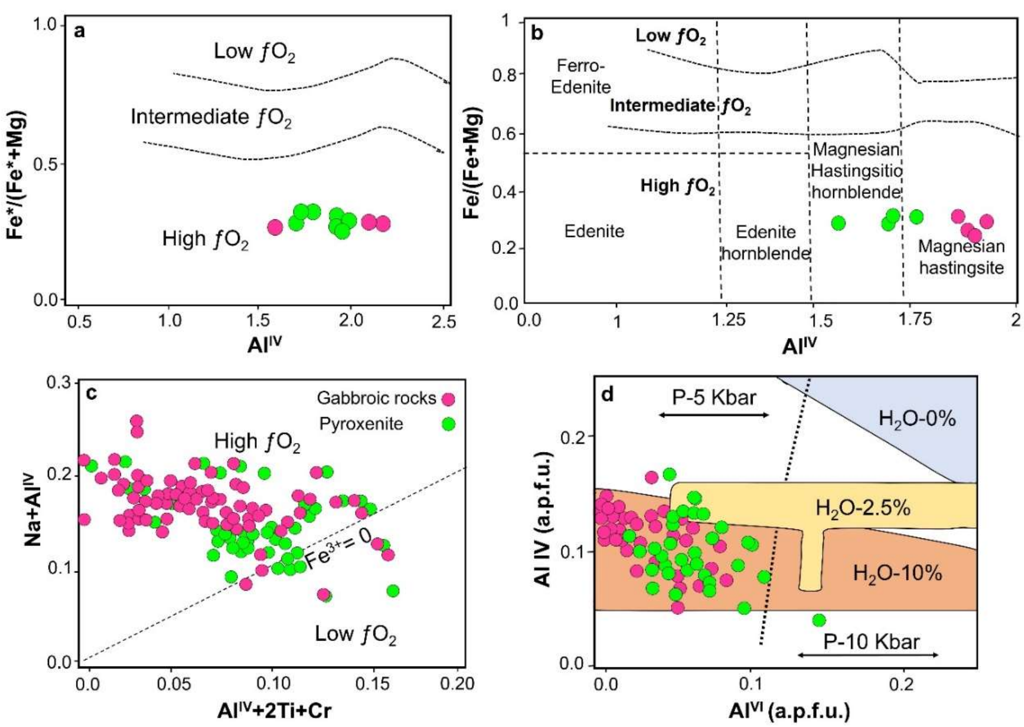


**Figure 8.** a) Amphibole samples of the XV deposit in the diagram proposed by Anderson and Smith (1995), b) Evaluation of oxygen fugacity using the chemical composition of amphiboles (Anderson and Smith, 1995), c) $Al^{VI}$+2Ti+Cr vs. Na+$Al^{IV}$ diagram for determination of oxygen fugacity (Schweitzer et al., 1979), and d) Al distribution diagram in tetrahedral and octahedral positions in pyroxenes in proportion to the amount percentage of magma $H_2O$ (Helz, 1973)

**Appendix Table e.** The results of electron microprobe analysis of ilmenite spots. The molar amount of ilmenite (Ilm) was calculated using (Anderson, 1968). The calculations are based on the number of 3 oxygen atoms

**Appendix Table f.** Electron microprobe analysis results for ilmenite and titanomagnetite type II for temperature and oxygen fugacity calculations. The molar amounts of ilmenite (Ilm) and Ulvospinel (Usp) were calculated using (Carmichael, 1967), (Anderson, 1968), (Lindsley & Spencer, 1982) and (Stormer, 1983) respectively. Calculations of temperature and oxygen fugacity are based on the calculation equation for $Fe^{3+}/Fe^{2+}$ and $FeO/Fe_2O_3$ using (Carmichael, 1967). The numbers in brackets are the number of analyses carried out for each pair of minerals

As pyroxene crystallization progresses, Al contents decrease with increasing $H_2O$ content. This trend is evident in Fig. 8d, where the magma is inferred to contain approximately 10 wt.% $H_2O$ at a pressure of 5 kbar. The presence of hydrous minerals, such as amphibole, indicates a magma source with elevated water content. The occurrence of amphibole in the studied rocks further supports the inference that the primary magma contained more than 3 wt.% $H_2O$ (e.g., Botcharnikov et al., 2008; Ridolfi et al., 2010; Howarth & Pearce, 2013). The $H_2O$ content of the magma was estimated from amphibole composition using equations (1) and (2) proposed by Ridolfi et al. (2010):

$$H_2O_{melt} = 5.215Al^{VI}*+12.28 \quad (1)$$

$$Al^{VI}*= Al^{VI}+(Al^{IV}/13.9) - ((Si+Ti)/5) - (^{C}Fe^{2+}/3) - (Mg/1.7) + ((^{B}Ca+^{A}\{\})/1.2) + (^{A}Na/2.7) - 1.5K - (Fe/1.6) \quad (2)$$

Based on the calculations, the magma contained between 0.13 and 5.24 wt. % $H_2O$, with an average of 2.29 wt. % during the crystallization of amphibole.

*Geothermometry and oxygen fugacity*

Geothermometry and oxygen fugacity calculations rely on the equilibrium between symbiotic oxide mineral pairs, such as ilmenite-hematite, titanomagnetite-ilmenite, or magnetite-ulvöspinel (Powell and Powell, 1977). The two key reactions that form the foundation for temperature and oxygen fugacity calculations in Fe-Ti oxide minerals are as follows (Powell & Powell, 1977):

$$FeTiO_3+Fe_3O_4 = Fe_2O_3+Fe_2TiO_4$$

$$6Fe_2TiO_4+O_2 = 6FeTiO_3+2Fe_3O_4$$

For Fe-Ti-O oxide mineralization systems, the equations outlined by Powell & Powell (1977) are applied for geothermometry and oxygen fugacity calculations. However, in the XV rock samples, elements such as Mn, Mg, V, Cr, and Al are incorporated into calculations using the equations from Carmichael (1967), Anderson (1968), Lindsley & Spencer (1982), Stormer (1983), as based on the equation from Spencer and Lindsley (1981). For reference, the QFM (quartz-fayalite-magnetite) buffer (Chou I-Ming, 1978) and the WM (wustite-magnetite) buffer (Eugster & Wones, 1962) are used for pressures below 1.5 kbar. The equilibrium temperature and oxygen fugacity were estimated for the ilmenite-titanomagnetite Type II co-growth mineral pair in the XV rock samples (Appendix Table f & Fig. 9a & b). Notably, there are variations in temperature and oxygen fugacity when using each of the reference equations (Carmichael, 1967; Anderson, 1968; Lindsley & Spencer, 1982; Stormer, 1983). In Figure 9a & b, the studied samples show an equilibrium temperature range of 448 to 727°C and variations in oxygen fugacity between -17.28 and -23.96 along the QFM buffer curve (Appendix Table) Oliver (1978), demonstrated that Ti-rich microcrystalline ilmenite and titanomagnetite minerals typically exhibit temperatures above 1000°C, while co-growths of ilmenite and titanomagnetite tend to show temperatures between 500 and 700°C. Additionally, co-growths of ilmenite and titanomagnetite, located between the QFM and MW buffer curves, have exhibited higher equilibrium temperatures (ranging from 500 to 740°C) and, as such, align along the ulvöspinel curve (Pasteris, 1985).

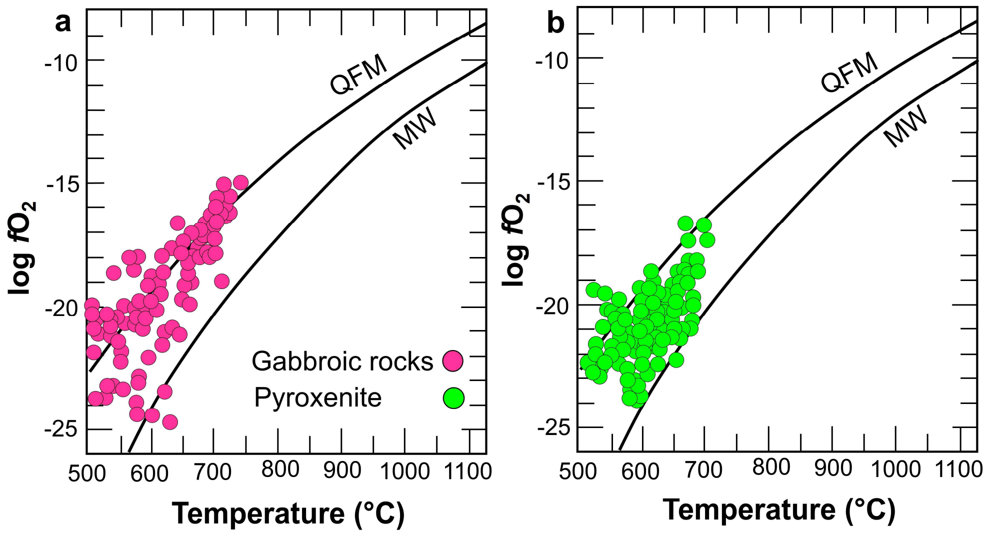


**Figure 9.** Estimation of temperature and oxygen fugacity using ilmenite and titanomagnetite oxide minerals shows the second type. The calculations are based on geothermometry equations (Spencer & Lindsley, 1981). The QFM (Chou I-Ming, 1978) and MW (Eugster & Wones, 1962) buffer curves are shown for reference and comparison at pressures less than 1.5 kbar

*Nature and Affinity of the Parental Magma*

The nature of the parental magma is closely linked to the composition of its crystallizing minerals (e.g., Avanzinelli et al., 2004). Alkaline amphiboles typically contain higher $Na_2O$, $TiO_2$, $K_2O$, and $Al_2O_3$ contents than subalkaline amphiboles (Molina et al., 2009). Amphiboles from the studied XV samples have $TiO_2$ contents ranging from 0.1 to 4.31 wt.%, $Al_2O_3$ contents from 3.79 to 16.14 wt.%, and Na2O contents from 0.47 to 2.89 wt.%. Based on the $TiO_2$ vs. $Al_2O_3$ diagram (Fig. 10a), the $Na_2O$ vs. $TiO_2$ diagram (Fig. 10b), and the MgO and $K_2O$ trends (not shown) of Molina et al. (2009), most amphiboles from both rock types plot within the alkaline field. Moreover, the $Al_2O_3$ vs. $SiO_2$ diagram for pyroxenes from both rock types in the XV intrusion (Fig. 10c; Le Bas, 1962) suggests an alkaline to subalkaline affinity for the parental magma.

Pyroxenes from the studied samples plot mainly within the alkali basalt field on the Ca + Na vs. Ti diagram (Fig. 10d; Leterrier et al., 1982). The Mg# values [Mg/(Mg + $Fe^{2+}$)], ranging from 0.749 to 0.892 with an average of 0.812, indicate a mantle-derived origin for the mafic–ultramafic magmatism of the XV rocks (Xie & Zhang, 1990; Huaimin et al., 2006). For further comparison and details, see Amraei et al. (2024a). The relatively high Mg# values of pyroxenes in the gabbroic and pyroxenitic units (Appendix Table a) suggest that the magmas were relatively primitive and possibly had a picritic affinity, likely generated by high degrees of partial melting in the mantle. The enrichment of alkaline elements in amphiboles ($Na_2O + K_2O > 3$ wt.%; Appendix Table b) further supports the alkaline affinity of the magma.

*Tectonic setting*

Coltorti et al. (2007) utilized amphibole chemistry in mantle xenoliths to discriminate between subduction-related and within-plate tectonic settings. Amphiboles from extensional environments (I-Amph) are characterized by higher $Na_2O$ and $SiO_2$ contents than those from subduction zones (S-Amph). On the $Na_2O$ versus $SiO_2$ diagram proposed by Coltorti et al. (2007) (Fig. 11a), most amphiboles from the XV intrusion fall within the extensional field, suggesting derivation from a mantle source related to an extensional or back-arc regime. Similarly, pyroxene chemistry plotted on the Ca vs. Ti + Cr diagram (Fig. 11b) supports an extensional magmatic affinity. According to the classification diagram of Nisbet and Pearce (1977) (Fig. 11c), most pyroxenes from the XV intrusion plot within the fields of within-plate tholeiitic basalts (WPT) and ocean-floor basalts (OFB), which are commonly associated with magmatic back-arc basins. The gabbroic and pyroxenitic varieties of the XV rocks show geochemical similarities to oceanic-crust pyroxenes from extensional zones of magmatic back-arc basins, as shown by the $Al_2O_3$ vs. Mg# [Mg# = 100 × Mg/(Mg + $Fe^{2+}$)] diagram (Fig. 11d; Rampone et al., 1998).

Geothermobarometric investigations of the XV gabbros and pyroxenites, together with regional studies across the Central Iranian Microcontinent and the PBB, suggest that fragments of the Iranian continental crust separated from Gondwana during the Early Cambrian breakup and later collided with Eurasia during the Triassic Cimmerian orogeny (e.g., Glennie, 2000; Nayebi et al., 2023). This crust experienced deformation, folding, and faulting during the Neoproterozoic as part of the Pan-African orogeny (550–600 Ma; Ramezani & Tucker, 2003). Magmatic and sedimentary activity in the PBB from the Late Neoproterozoic to Early Cambrian has been related to crustal thinning and extension associated with intracontinental rifting (Berberian & King, 1981). Berberian and King (1981) proposed that the final stages of the Pan-African orogeny in the Arabian–Iranian Shield (ca. 686–517 Ma) initiated post-orogenic extensional magmatism within the PBB, whereas Talbot and Alavi (1996) suggested that an intracontinental rift began to develop in this domain during the Late Neoproterozoic–Early Cambrian.

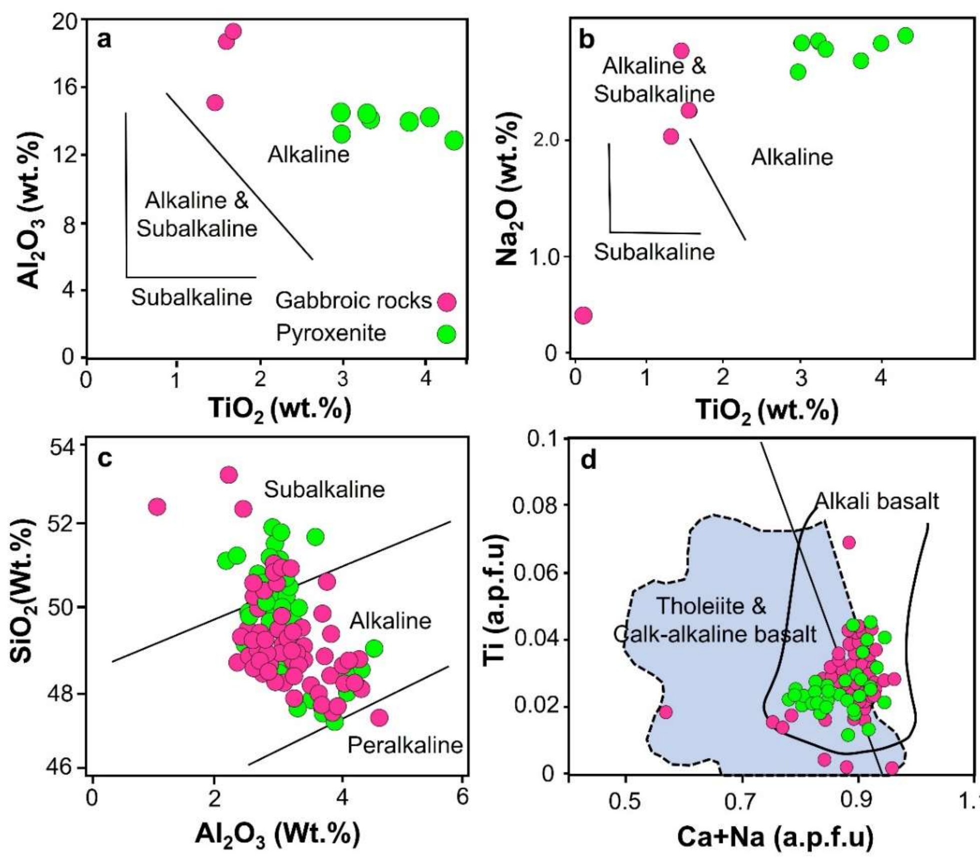


**Figure 10.** a and b) $TiO_2$ vs. $Al_2O_3$, $Na_2O$ based on amphibole chemistry (Molina et al., 2009); c) Diagram of $SiO_2$-$Al_2O_3$ based on pyroxene chemistry (Le Bas, 1962), and d) Ca+Na vs. Ti diagram for discriminate of nature of magma (Leterrier et al., 1982)

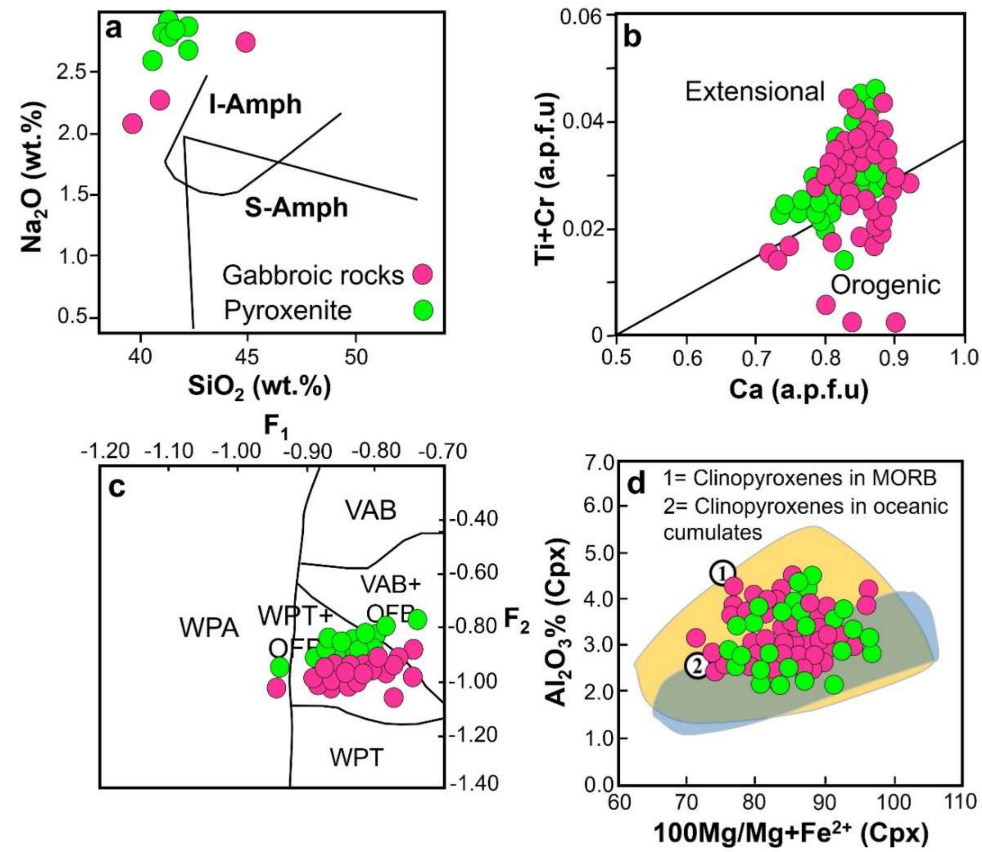


**Figure 11.** a) Location of amphiboles of gabbroic and pyroxenitic rocks in the diagram of $SiO_2$ vs. $Na_2O$ (Coltorti et al., 2007), (I-Amph: within-plate amphiboles; S-Amph: Supra-subduction amphiboles); b) Diagram of Ti+Cr vs. Ca (Leterrier et al., 1982); c) Chemical composition of pyroxene in F1 vs. F2 tectonic setting diagram (Nisbet and Pearce, 1977). F1= - (0.012 * $SiO_2$) - (0.0807 * $TiO_2$) + (0.0026 * $Al_2O_3$) - (0.0012 * $FeO_t$) - (0.0026 * MnO) + (0.0087 * MgO) - (0.0128 * CaO) - (0.0419 * $Na_2O$) and F2= - (0.0149 * $SiO_2$) - (0.0818 * $TiO_2$) + (0.0212 * $Al_2O_3$) - (0.0041 * $FeO_t$) - (0.1435 * MnO) + (0.0029 * MgO) - (0.0085 * CaO) - (0.016 * $Na_2O$), and d) Diagram of Rampone et al. (1998)

Subsequent studies have refined this interpretation and identified the Bafq region and the Posht-e-Badam zone as a continental back-arc extensional province located along the northern margin of Gondwana during Early Paleozoic time (e.g., Rajabi et al., 2012, 2015; Amraei et al., 2020, 2024a, b, 2025). Although a back-arc basin model for the Bafq region has previously been proposed, the present study provides a more integrated geochemical, mineralogical, and geothermobarometric dataset that better constrains the mantle and magmatic processes responsible for melt generation. Amphibole and pyroxene data from the XV intrusion, together with the chemistry of Fe–Ti oxide and phosphate minerals, indicate that the XV magma originated from hydrous, oxidized mantle melts generated by partial melting of metasomatized upper-mantle peridotites beneath an extensional back-arc environment. These melts were likely influenced by slab-derived fluids and asthenospheric influx during rifting along the northern Gondwanan margin in relation to the Proto-Tethyan subduction system (e.g., Pearce, 2008; Richards, 2015).

The integration of these new petrochemical data with previous tectonic frameworks reinforces the interpretation that the Bafq–Posht-e-Badam region evolved as a continental back-arc basin affected by asthenospheric upwelling and lithospheric stretching. This geodynamic setting resembles other peri-Gondwanan extensional systems, such as the Arabian–Nubian Shield (Stoeser & Frost, 2006) and the Himalaya–Karakoram domain (Richards, 2015), where lithospheric thinning following slab rollback led to mafic magmatism with comparable chemical signatures. Structural and gravity data (Rajabi et al., 2012) support progressive rifting and extensional subsidence in the Bafq–Posht-e-Badam corridor, producing NW–SE-trending grabens and mafic intrusions aligned with inherited extensional structures.

Zircon U–Pb ages reported by Ramezani and Tucker (2003) confirm that the Central Iranian Microcontinent was once part of Gondwana along its northern margin and that magmatism in the PBB was broadly synchronous with early back-arc extension. Amraei et al. (2020, 2024b) demonstrated that the mafic and ultramafic rocks of the XV intrusion originated from subduction-modified mantle peridotites. This magmatic event represents early back-arc magmatism linked to crustal extension and partial melting of metasomatized upper mantle beneath the Proto-Tethyan subduction margin. Progressive asthenospheric upwelling beneath this region shifted the tectonic regime from compression to extension, facilitating the ascent of mantle-derived melts and the emplacement of the XV intrusive complex (Fig. 12).

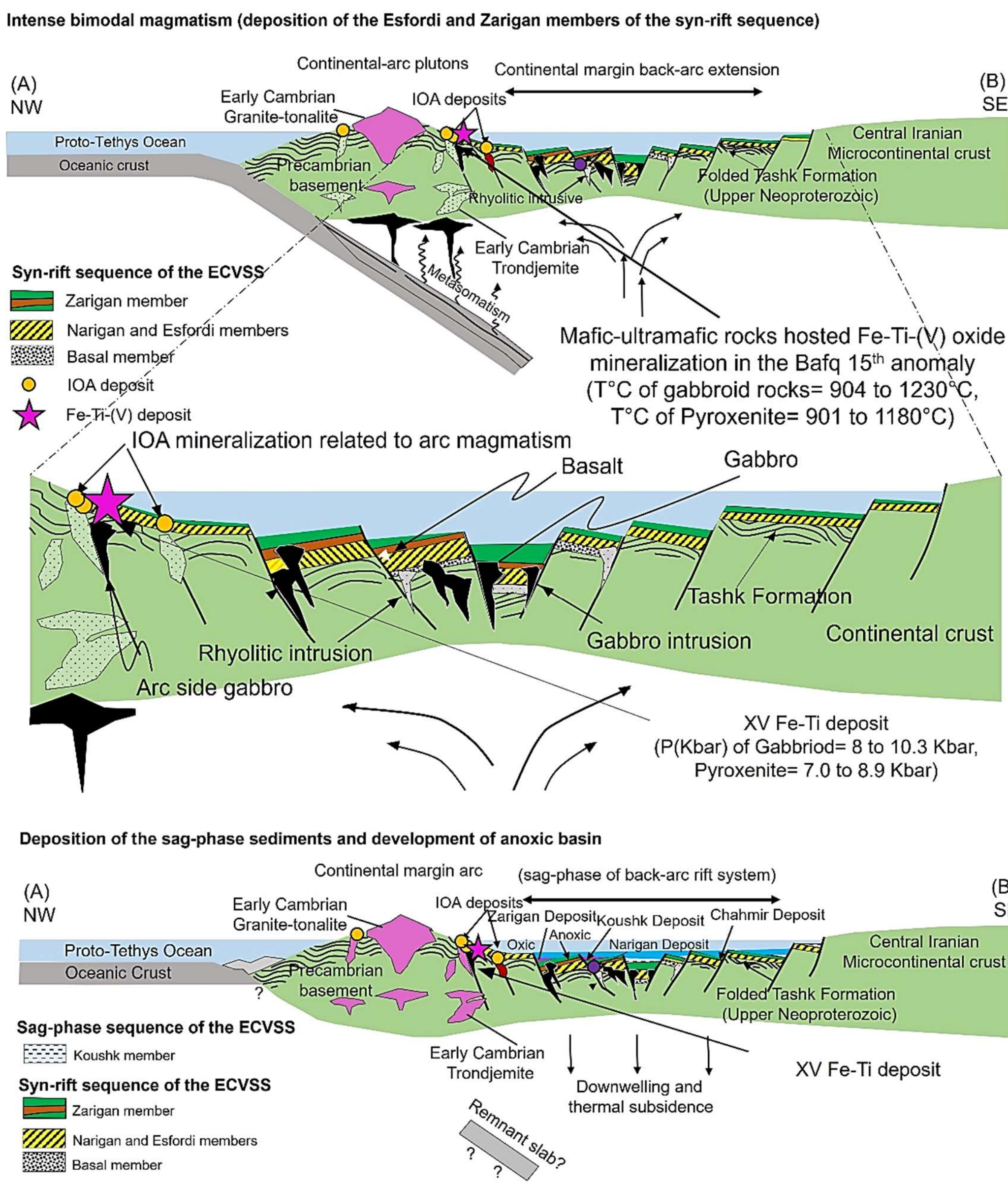


**Figure 12.** Schematic tectonic model of the Fe-Ti-P oxide mineralization at XV deposit in the central Iranian subcontinent and the Posht-e-Badam block in a Late Neoproterozoic-Lower Cambrian extensional back-arc basin (Modified after Rajabi et al, 2015)

The presence of amphibole, ilmenite, and titanomagnetite in the XV rocks indicates formation under high oxygen fugacity, implying an oxidized magmatic environment (Amraei et al., 2024a, 2025). High oxygen fugacity, elevated magmatic $H_2O$ contents, and abundant Fe–Ti ± P in the parental melt constitute key petrogenetic factors that promoted mineralization within the XV intrusion. Such characteristics are common in back-arc magmas influenced by slab-derived fluids, where oxidized and hydrous conditions enhance differentiation and ore formation (Richards, 2015). Fractional crystallization in relatively deep magma chambers of this back-arc system produced evolved Fe–Ti ± P-bearing gabbroic rocks consistent with extensional magmatism. The combined evidence from mineral chemistry, thermobarometry, structural analysis, and geochemical modeling therefore indicates that the XV intrusion and its associated gabbroic–pyroxenitic series were generated by mantle melting beneath a continental back-arc extensional setting. This interpretation integrates previous tectonic models (e.g., Berberian & King, 1981; Talbot & Alavi, 1996; Rajabi et al., 2012, 2015) with new geochemical and mineralogical data, demonstrating that magmatic differentiation and mantle dynamics within the Bafq–Posht-e-Badam region represent an advanced stage of extensional evolution following the Pan-African orogeny. Consequently, the XV intrusion refines our understanding of the northern Gondwanan margin as a transitional zone where subduction-related and intracontinental extensional processes interacted to generate hydrous, oxidized mafic magmatism and associated ore-forming systems.

## Conclusions

The Fe-Ti oxide ± P mineralization at the XV deposit formed within gabbroic and pyroxenitic rocks containing plagioclase, clinopyroxene, amphibole, and apatite as the principal mineral assemblage. The chemical composition of clinopyroxene and amphibole defines an alkaline to calc-alkaline magmatic affinity, reflecting magma evolution in a back-arc extensional rift basin. Amphibole chemistry enriched in $Na_2O$ and $SiO_2$, together with the geochemical traits of pyroxene, indicates formation from a hydrous and oxidized mantle-derived melt influenced by slab-related fluids under an extensional regime. Thermobarometric calculations reveal that gabbros crystallized at temperatures of 904-1230 °C and pressures of 8.0-10.3 kbar, while pyroxenites formed at 901-1180 °C and 7.0-8.9 kbar. Temperatures estimated from ilmenite-titanomagnetite equilibria range between 448 and 727 °C, with most values clustering around 554-645 °C and the highest values (703-727 °C) corresponding to the gabbroic facies. The close agreement among amphibole-pyroxene and oxide geothermometers, together with redox indicators, points to the crystallization of oxidizing, hydrous melts at deep crustal levels and subsequent cooling in an evolving magma chamber, where fractional crystallization concentrated the Fe-Ti ± P phases. Integration of mineral chemistry, thermobarometric, and tectonomagmatic relationships documents a progressive transition from a compressional to a transitional extensional regime, contemporaneous with asthenospheric upwelling and lithospheric stretching along the continental margin that facilitated magma ascent and emplacement. Thus, the XV intrusion represents a refined stage of continental back-arc magmatism, generated by crustal thinning, mantle melting, and the ascent of hydrous, oxidized mafic magma from a hypabyssal mantle source. Altogether, the mineralogical, geochemical, and thermal evidence demonstrates that the XV deposit is a product of mantle melting and magma differentiation under oxidizing, volatile rich conditions in a continental back-arc environment, refining the understanding of extensional magmatism by constraining the depth, temperature, and redox state of magma emplacement and by illustrating the petrogenetic link between mafic melts and Fe-Ti ± P mineralization during the tectonic transition from compressional to extensional regimes.

**Acknowledgment**

This study is part of a Ph.D. thesis by S. Amraei at the Shahid Beheshti University, Tehran, Iran.

**Conflict of interest**

The authors declare that they have no known competing financial interests or personal relationships that could have appeared to influence the work reported in this paper. The manuscript has been prepared to conform to the instructions for contributors. This material has not been previously published elsewhere, nor is it under consideration for publication elsewhere. All the authors have approved this submission. There are no closely related manuscripts that have been submitted or are in press. As far as I am aware, there are no actual or potential conflicts of interest, of a financial, personal or other kind, with other people or organizations that could inappropriately influence, or be perceived to influence, this work. No funding source has had any involvement in the study design, collection, analysis and interpretation of the data, in the writing of the manuscript and in the decision to submit the paper for publication.

**Dear Editor-in-Chief Journal of Geopersia,**

I confirm that all persons who meet authorship criteria are listed as authors, and they certify that they have participated sufficiently in the work to take public responsibility for the content, including participation in the concept, design, analysis, writing, or revision of the manuscript. Sakine Amraei: Conceptualization, writing - original draft, data manipulation. Majid Ghasemi Siani and Hamed Ebrahimi Fard: writing (review and editing) and project administration. Mehrdad Behzadi and Mohammad Yazdi: Data collection and manipulation, assisted with fieldwork and writing (review and editing). Liang Qiu, Chang-Zhi Wu, Minghua Ren and Shahrokh Rajabpour: Provided resources and writing (review and editing).

**References**

Aoki, K. I., Shiba, I., 1973. Pyroxenes from lherzolite inclusions of Itinome-gata, Japan. Lithos, 6(1): 41-51Anderson, A. T., 1968. Oxidation of the LaBlache Lake titaniferous magnetite deposit, Quebec. The Journal of Geology, 76(5): 528-547.

Andersen, D. J., Lindsley, D. H., 1988. Internally consistent solution models for Fe-Mg-Mn-Ti oxides; Fe-Ti oxides. American Mineralogist, 73(7-8): 714-726.

Anderson, J. L., Smith, D. R., 1995. The effects of temperature and $fO_2$ on the Al-in-hornblende barometer. American mineralogist, 80(5-6): 549-559.

Avanzinelli, R., Bindi, L., Menchetti, S., Conticelli, S., 2004. Crystallization and genesis of peralkaline magmas from Pantelleria Volcano, Italy: an integrated petrological and crystal-chemical study. Lithos, 73(1-2): 41-69.

Aghanabati, S. A., 2013. Geology of Iran. Geological Survey of Iran, pp. 587 (in Persian).

Amraei, S., Behzadi, M., Yazdi, M., Kouhestani, H., Ghasemi Siani, M., 2021. Ti-Fe mineralization in Bafq anomaly no. 15, Central Iran: Insights to mineralogy and mineral chemistry. Petrological Journal, 12(1): 93-112 (in Persian).

Amraei, S., Ghasemi Siani, M., Yazdi, M., Qiu, L., Moine, B., Ren, M., 2024a. Fe-Ti oxide mineralization in the XV intrusion, Bafq mining district, Central Iran: insights from mineralogy, mineral chemistry and S isotopic data. Journal of Earth Science, 35 (5): 1704-1719.

Amraei, S., Yazdi, M., Qiu, L., Wu, C. Z., Chen, L., Moine, B., Rajabpour, S., 2024b. Apatite U-Pb geochronology and whole rock, Sr-Nd-Pb isotopic geochemistry of XV mafic-ultramaf
ic intrusion, Bafq, Central Iran: Implications for petrogenesis and tectonic setting. Island Arc, 33(1): e12514.

Amraei, S., Siani, M.G., Yazdi, M., Qiu, L., Wu, C.Z., Ren, M. and Rajab pour, S., 2025. Apatite chemistry from the XV IOA deposit, the Bafq-Saqand Metallogenic Province (BSMP), Central Iran: constrains on the genesis of IOA deposits. Turkish Journal of Earth Sciences, 34(4): 532-547.

Buddington, A. F., Lindsley, D. H., 1964. Iron-titanium oxide minerals and synthetic equivalents. Journal of petrology, 5(2): 310-357.

Bishop, F.C., 1980. The distribution of $Fe^{2+}$ and Mg between coexisting ilmenite and pyroxene with application to geothermometry. American Journal of Sciences, 280(1): 46-77.

Berberian, M., King, G. C. P., 1981. Towards a paleogeography and tectonic evolution of Iran. Canadian journal of earth sciences, 18(2): 210-265.

Blevin, P. L., Chappell, B. W., Allen, C. M., 1996. Intrusive metallogenic provinces in eastern Australia based on granite source and composition.

Barclay, J., Carmichael, I. S. E., 2004. A hornblende basalt from western Mexico: water-saturated phase relations constrain a pressure-tempera window of eruptibility. Journalture of Petrology, 45(3): 485-506.

Botcharnikov, R. E., Koepke, J., Holtz, F., McCammon, C., Wilke, M., 2005. The effect of water activity on the oxidation and structural state of Fe in a ferro-basaltic melt. Geochimica et Cosmochimica Acta, 69(21): 5071-5085.

Berger, J., Femenias, O., Mercier, J.C.C. and Demaiffe, D., 2005. Ocean-floor hydrothermal metamorphism in the Limousin ophiolites (western French Massif Central): evidence of a rare preserved Variscan oceanic marker. journal of Metamorphic geology, 23(9): 795-812.

Blundy, J., Cashman, K., 2008. Petrologic reconstruction of magmatic system variables and processes. Reviews in Mineralogy and Geochemistry, 69(1): 179-239.

Botcharnikov, R.E., Almeev, R.R., Koepke, J. and Holtz, F., 2008. Phase relations and liquid lines of descent in hydrous ferrobasalt—implications for the Skaergaard intrusion and Columbia River flood basalts. Journal of Petrology, 49(9):1687-1727.

Brzozowski, M. J., Good, D. J., Wu, C., Li, W., 2021. Iron isotope fractionation during sulfide liquid evolution in Cu-PGE mineralization of the Eastern Gabbro, Coldwell Complex, Canada. Chemical Geology, 576: 120282.

Carmichael, I. S., 1967. The mineralogy and petrology of the volcanic rocks from the Leucite Hills, Wyoming. Contributions to Mineralogy and Petrology, 15: 24-66.

Chou, I. M., 1978. Calibration of oxygen buffers at elevated P and T using the hydrogen fugacity sensor. American Mineralogist, 63(7-8): 690-703.

Coltorti, M., Bonadiman, C., Faccini, B., Grégoire, M., O'Reilly, S.Y., Powell, W., 2007. Amphiboles from supra subduction and intraplate lithospheric mantle. Lithos, 99(1-2): 68-84.

Daliran, F., Stosch, H. G., Williams, P., Jamali, H., Dorri, M. B., Corriveau, L., Mumin, A. H., 2010. Early Cambrian iron oxide-apatite-REE (U) deposits of the Bafq district, east-central Iran. Exploring for iron oxide copper-gold deposits: Canada and global analogues. Geologists Association, Canada, 143-155.

Eugster, H. P., Wones, D. R., 1962. Stability relations of the ferruginous biotite, annite. Journal of Petrology, 3(1): 82-125.

Ewart, A., 1979. A review of the mineralogy and chemistry of Tertiary-Recent dacitic, latitic, rhyolitic, and related salic volcanic rocks. Developments in Petrology, 6: 13-121.

Ghazi, J. M., Moazzen, M., 2020. Reply to discussion by A. Aftabi and S. Mohseni on "Combined igneous and hydrothermal source for the Kiruna-type Bafq magnetite-apatite deposits in Central Iran; trace element and oxygen isotope studies of magnetite" by Mehdipour Ghazi et al,. [Ore Geology Reviews 105 (2019) 590-604]. Ore Geology Reviews, 125: 103416.

Ghiorso, M. S., Sack, O., 1991. Fe-Ti oxide geothermometry: thermodynamic formulation and the estimation of intensive variables in silicic magmas. Contributions to Mineralogy and Petrology, 108: 485-510.

Glennie, K. W., 2000. Cretaceous tectonic evolution of Arabia's eastern plate margin: a tale of two oceans.

Ghiorso, M. S., Evans, B. W., 2008. Thermodynamics of rhombohedral oxide solid solutions and a revision of the Fe-Ti two-oxide geothermometer and oxygen-barometer. American Journal of science, 308(9): 957-1039.

Hynes, A., 1982. A comparison of amphiboles from medium and low-pressure metabasites.

Contributions to Mineralogy and Petrology, 81(2): 119-125.
Hammarstrom, J. M., Zen, E. A., 1986. Aluminum in hornblende: an empirical igneous geobarometer. American mineralogist, 71(11-12): 1297-1313.
Haggerty, J. A., 1991. Evidence from fluid seeps atop serpentine seamounts in the Mariana Forearc: Clues for emplacement of the seamounts and their relationship to fore arc tectonics. Marine Geology, 102(1-4): 293-309.
Helmy, H. M., Ahmed, A. F., El Mahallawi, M. M., Ali, S. M., 2004. Pressure, temperature and oxygen fugacity conditions of calc-alkaline granitoids, Eastern Desert of Egypt, and tectonic implications. Journal of African Earth Sciences, 38(3): 255-268.
Hawthorne, F.C., Oberti, R., Harlow, G.E., Maresch, W.V., Martin, R.F., Schumacher, J.C., Welch, M.D., 2012. Nomenclature of the amphibole supergroup. American Mineralogist, 97(11-12): 2031-2048.
Helz, R. T., 1973. Phase relations of basalts in their melting range at $PH_2O$= 5 kb as a function of oxygen fugacity: part I. Mafic phases. Journal of Petrology, 14(2): 249-302.
Huaimin X., Shuwen D., Ping, J., 2006. Mineral chemistry' geochemistry and U-Pb SHRIMP zircon data of the Yangxin monzonitic intrusive in the foreland of the Dabie orogen science in China", Earth Sciences, 49: 684-695.
Howarth, G. H., Pearce, S. A., 2013. Hydration Vs. Oxidation: Modelling Implications for Fe-Ti Oxide Crystallisation in Mafic Intrusions, with Specific Reference to the Panzhihua Intrusion, SW China. Geoscience Frontiers, 4(5): 555-569.
Heidarian, H., Alirezaei, S. and Lentz, D.R., 2018. Chadormalou Kiruna-type magnetite-apatite deposit, Bafq district, Iran: Insights into hydrothermal alteration and petrogenesis from geochemical, fluid inclusion, and sulfur isotope data. Ore Geology Reviews, 83: 43-62.
Johnson, M. C., Rutherford, M. J., 1989. Experimental calibration of the aluminum-in-hornblende geobarometer with application to Long Valley caldera (California) volcanic rocks. Geology, 17(9): 837-841.
Jugo, P. J., Candela, P. A., Piccoli, P. M., 1999. Magmatic sulfides and Au: Cu ratios in porphyry deposits: an experimental study of copper and gold partitioning at 850 C, 100 MPa in a haplogranitic melt-pyrrhotite-intermediate solid solution-gold metal assemblage, at gas saturation. Lithos, 46(3): 573-589.
Kretz, R., 1994. Metamorphic crystallization. John Wiley and Sons Ltd, New York, USA, 507 pp.
Khedr, M.Z., Takazawa, E., Arai, S., Stern, R.J., Morishita, T., El-Awady, A., 2022. Styles of Fe-Ti-V ore deposits in the Neoproterozoic layered mafic-ultramafic intrusions, south Eastern Desert of Egypt: Evidence for fractional crystallization of V-rich melts. Journal of African Earth Sciences 194, 104620.
Le Bas, M. J., 1962. The role of aluminum in igneous clinopyroxenes with relation to their parentage. American Journal of Science, 260(4): 267-288.
Leterrier, J., Maury, R. C., Thonon, P., Girard, D. and Marchal, M., 1982. Clinopyroxene composition as a method of identification of the magmatic affinities of paleo-volcanic series. Earth and Planetary Science Letters, 59(1): 139-154.
Lindsley, D. H., Spencer, K. J., 1982. Fe-Ti oxide geothermometry: Reducing analyses of coexisting Ti-magnetite (Mt) and ilmenite (Ilm). EOS Transactions, American Geophysical Union, 63(18): 471.
Lindsley, D. H., Frost, B. R., 1992. Equilibria among Fe-Ti oxides, pyroxenes, olivine, and quartz: Part I. Theory. American Mineralogist, 77(9-10): 987-1003.
Lepage, L. D., 2003. ILMAT: an Excel worksheet for ilmenite-magnetite geothermometry and geobarometry. Computers and Geosciences, 29(5), 673-678.
Lattard, D., Sauerzapf, U., Käsemann, M., 2005. New calibration data for the Fe-Ti oxide thermo-oxybarometers from experiments in the Fe-Ti-O system at 1 bar, 1,000-1,300 C and a large range of oxygen fugacities. Contributions to Mineralogy and Petrology, 149: 735-754.
Morimoto, N., 1988. Nomenclature of pyroxenes. Canadian Mineralogist, 27: 143-156.
Molina, J. F., Scarrow, J. H., Montero, P. G., Bea, F., 2009. High-Ti amphibole as a petrogenetic indicator of magma chemistry: evidence for mildly alkalic-hybrid melts during the evolution of Variscan basic-ultrabasic magmatism of Central Iberia. Contributions to Mineralogy and Petrology, 158: 69-98.
Murphy, J. B., Blais, S. A., Tubrett, M., McNeil, D., Middleton, M., 2012. Microchemistry of

amphiboles near the roof of a mafic magma chamber: Insights into high level melt evolution. Lithos, 148: 162-175.

Mutch, E. J. F., Blundy, J. D., Tattitch, B. C., Cooper, F. J., Brooker, R. A., 2016. An experimental study of amphibole stability in low-pressure granitic magmas and a revised Al-in-hornblende geobarometer. Contributions to Mineralogy and Petrology, 171: 1-27.

Mokchah, N., Mathieu, L., 2022. Origin and evolution of the iron-rich upper unit and Fe-Ti-V mineralization of the Neoarchean Lac Doré layered intrusion, Chibougamau, Québec. Journal of Petrology, 63(3): egac006.

Nisbet, E.G., Pearce, J.A., 1977. Clinopyroxene composition in mafic lavas from different tectonic settings. Contributions to Mineralogy and Petrology, 63(2): 149-160.

Nekvasil, H., 1992. Ternary feldspar crystallization in high-temperature felsic magmas. American Mineralogist, 77(5-6): 592-604.

Nayebi, N., Esmaeily, D., Shinjo, R., Deevsalar, R., Modabberi, S., Lehmann, B., 2023. Petrogenetic and geodynamic evolution of plutonic rocks from the Chadormalu district, Kashmar-Kerman tectonic zone, Central Iran. Mineralogy and Petrology, 1-19.

Oliver, G. J., 1978. Ilmenite-magnetite geothermometry and oxygen barometry in granulite and amphibolite facies gneisses from Doubtful Sound, Fiorland, New Zealand. Lithos, 11(2), 147-153.

Powell, R., Powell, M., 1977. Geothermometry and oxygen barometry using coexisting iron- titanium oxides: a reappraisal. Mineralogical Magazine, 41(318): 257-263.

Pasteris, J. D., 1985. Relationships between temperature and oxygen fugacity among Fe-Ti oxides in two regions of the Duluth Complex. The Canadian Mineralogist, 23(1): 111-127.

Petrik, I., Nabelek, P. I., Janak, M., Plasienka, D., 2003. Conditions of formation and crystallization kinetics of highly oxidized pseudotachylytes from the High Tatras (Slovakia). Journal of Petrology, 44(5): 901-927.

Putirka, K. D., 2008. Thermometers and barometers for volcanic systems. Reviews in mineralogy and geochemistry, 69(1): 61-120.

Putirka, K., 2016. Rates and styles of planetary cooling on Earth, Moon, Mars, and Vesta, using new models for oxygen fugacity, ferric-ferrous ratios, olivine-liquid Fe-Mg exchange, and mantle potential temperature. American Mineralogist, 101(4) 819-840.

Poshtkoohi, M., Ahmad, T., Choudhary, A. K., 2018. Geochemistry and petrogenesis of Biabanak-Bafq mafic magmatism: Implication for the evolution of central Iranian terrane. Journal of Earth System Science, 127: 1-30.

Rutter, M. J., Van der Laan, S. R., Wyllie, P. J., 1989. Experimental data for a proposed empirical igneous geobarometer: aluminum in hornblende at 10 kbar pressure. Geology, 17(10): 897-900.

Rampone, E., Hofmann, A.W., Raczek, I., 1998. Isotopic contrasts within the Internal Liguride ophiolite (N. Italy): the lack of a genetic mantle-crust link. Earth and Planetary Science Letters, 163(1-4):175-189.

Ramezani, J. and Tucker, R. D., 2003. The Saghand region, central Iran: U-Pb geochronology, petrogenesis and implications for Gondwana tectonics. American journal of science, 303(7): 622-665.

Ridolfi, F., Renzulli, A., Puerini, M., 2010. Stability and chemical equilibrium of amphibole in calc-alkaline magmas: an overview, new thermobarometric formulations and application to subduction-related volcanoes. Contributions to Mineralogy and Petrology, 160: 45-66.

Ridolfi, F., Renzulli, A., 2012. Calcic amphiboles in calc-alkaline and alkaline magmas: thermobarometric and chemometric empirical equations valid up to 1,130° C and 2.2 GPa. Contributions to Mineralogy and Petrology, 163: 877-895.

Rajabi, A., Rastad, E., Canet, C., 2012. Metallogeny of Cretaceous carbonate-hosted Zn-Pb deposits of Iran: geotectonic setting and data integration for future mineral exploration. International Geology Review, 54(14): 1649-1672.

Rajabi, A., Canet, C., Rastad, E., Alfonso, P., 2015. Basin evolution and stratigraphic correlation of sedimentary-exhalative Zn-Pb deposits of the Early Cambrian Zarigan-Chahmir Basin, Central Iran. Ore Geology Reviews, 64: 328-353.

Richards, J. P., 2015. Tectonic, magmatic, and metallogenic evolution of the Tethyan orogen: From subduction to collision. Ore Geology Reviews, 70, 323-345.

Schweitzer, E. L., Papike, J. J., Bence, A. E., 1979. Statistical analysis of clinopyroxenes from deep-sea

basalts. American Mineralogist, 64(5-6): 501-513.
Stormer, J. C., 1983. The effects of recalculation on estimates of temperature and oxygen fugacity from analyses of multicomponent iron-titanium oxides. American Mineralogist, 68(5-6): 586-594.
Schmidt, M. W., 1992. Amphibole composition in tonalite as a function of pressure: an experimental calibration of the Al-in-hornblende barometer. Contributions to mineralogy and petrology, 110(2-3): 304-310.
Soesoo, A., 1997. A multivariate statistical analysis of clinopyroxene composition: Empirical coordinates for the crystallization P-T estimations. Geological Society of Sweden (Geologiska Foreningen), 119(1): 55-60.
Scaillet, B., Evans, B.W., 1999. The 15 June 1991 eruption of Mount Pinatubo. I. Phase equilibria and pre-eruption P-T-$fO_2$-$fH_2O$ conditions of the dacite magma. Journal of Petrology, 40(3): 381-411.
Stein, E., Dietl, C., 2001. Hornblende thermobarometry of granitoids from the Central Odenwald (Germany) and their implications for the geotectonic development of the Odenwald. Mineralogy and petrology, 72: 185-207.
Stoeser, D. B., Frost, C. D., 2006. Nd, Pb, Sr, and O isotopic characterization of Saudi Arabian shield terranes. Chemical Geology, 226 (3-4), 163-188.
Talbot, C. J., Alavi, M., 1996. The past of a future syntaxis across the Zagros. Geological Society, London, Special Publications, 100(1): 89-109.
Wones, D.R., 1989. Significance of the assemblage titanite+ magnetite+ quartz in granitic rocks. American Mineralogist, 74(7-8): 744- 749.
Wan, B., Xiao, W., Windley, B. F., Yuan, C., 2013. Permian hornblende gabbros in the Chinese Altai from a subduction-related hydrous parent magma, not from the Tarim mantle plume. Lithosphere, 5(3): 290-299.
Xie, Y.W., Zhang Y.Q., 1990. Peculiarities and genetic significance of hornblende from granite in the Hengduansan region. Acta Mineral Sin, 10: 35-45.
Yan, S., Shan, Q., Niu, H.C., Yang, W.B., Li, N.B., Zeng, L.J., Jiang, Y.H., 2015. Petrology and geochemistry of late Carboniferous hornblende gabbro from the Awulale Mountains, western Tianshan (NW China): Implication for an arc- nascent back-arc environment. Journal of Asian Earth Sciences, 113: 218-237.
Yavuz, F., Döner, Z., 2017. WinAmptb: A Windows program for calcific amphibole thermobarometry. Periodico di Mineralogia, 86(2): 135-167.